Laboratori Nazionali di Legnaro (Istituto Nazionale di Fisica Nucleare)

Presented as poster (4th Oct) at NIBS2022, 2-7 Oct 2022, Padua, Italy

Observation of beamlet displacement and parallelism in NIO1

M. Ugoletti[1,2], M. Cavenago[1], R. Agnello[2], M. Barbisan[2], R. Delogu[2], A. Pimazzoni[2], C. Poggi[2]

[1)] INFN-LNL, viale dell'Università 2, 35020 Legnaro (PD), Italy; [2)] Consorzio RFX (CNR,ENEA,INFN,UNIPD,Acciaierie Venete SpA) Corso Stati Uniti 4, 35127 Padova, Italy

Abstract: The compact radiofrequency negative ion source NIO1 (Negative Ion Optimization phase 1) has many available CF40 ports for side views of beamlet matrix. Two kinds of deflecting magnetic systems are present, namely the fringe field of the source filter Bs (mostly directed in x direction where z is beam extraction direction) and the electron deflection filter B^d (due to magnets inserted in the extraction grid EG and the post-acceleration grid PA) mostly directed in the y direction. Their effect can be separated by cameras looking from different directions, namely CAM1 (looking from –x axis) is sensitive to B^s while CAM2 (looking from –y axis) verifies B^d effect; both cameras are also sensitive to beam optics, dependent on extracted beamlet currents, their uniformity and applied voltage. Optional algorithms for noise rejection and pre-smoothing can improve automatic recognizing of beamlet peaks, while a good fraction of images can be simply fitted by Gaussian shapes. This analysis allows to estimate beamlet displacement and deflection. Typical shapes of extracted beamlets are listed, noting in CAM2 the effect of B^d_y sign reversal (due to EG magnets) and of the compensation techniques used to obtain beamlet parallelism (in good matching); systematic analysis of correlation between images, other source measurements and simple beam simulation is also attempted. Alignment and scaling of images is discussed also with reference to background objects. Moreover, beamlet convergence was sometimes observed, and corresponding datasets were tagged for optics correction. Finally beam size information useful for Faraday cup design is obtained.

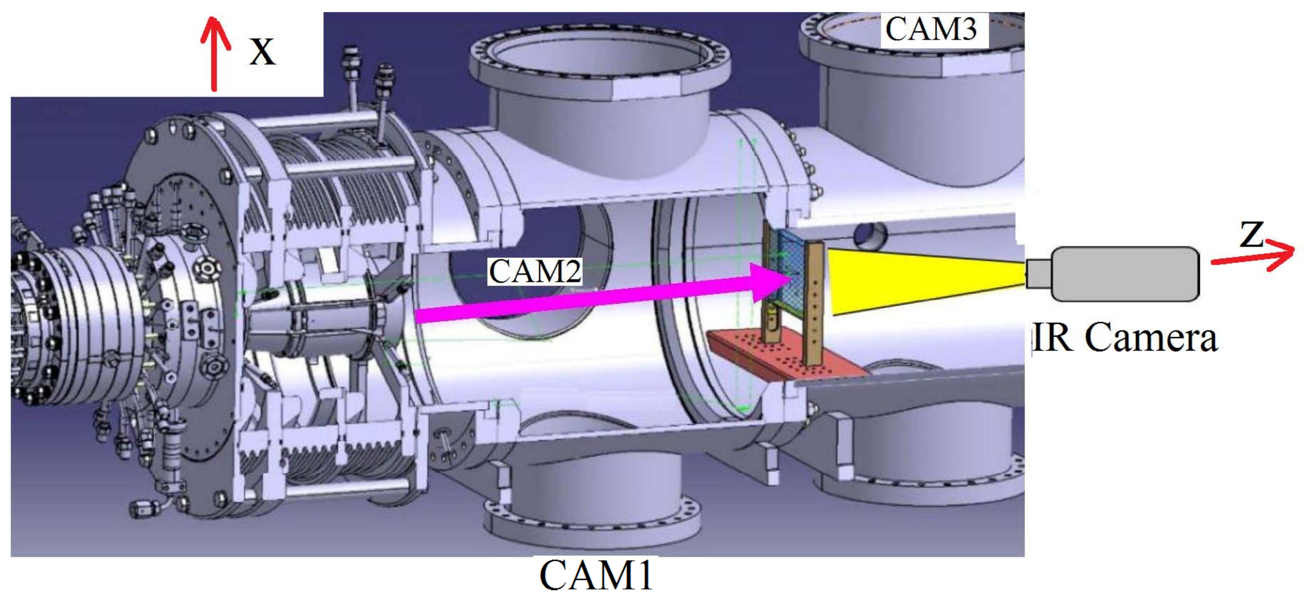

Figure 1. Overall 3D cut view, showing part of NIO1 accelerating electrodes; note CAM1, CAM2 and CAM3 placement; CFC tile recently moved after CAM3 position

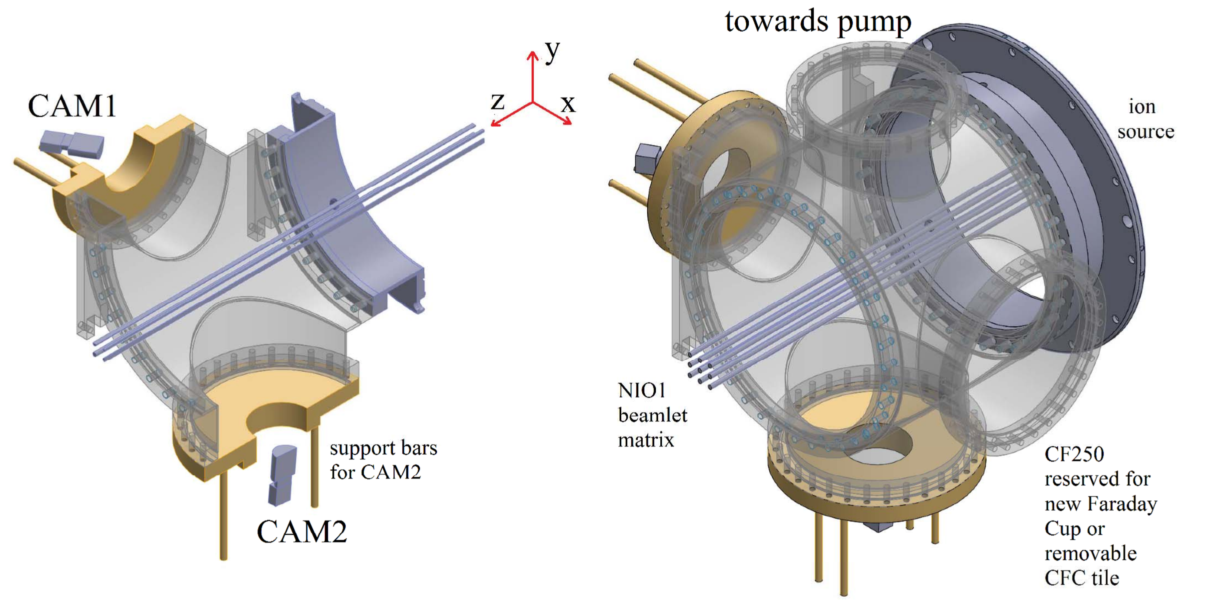

Some notation:
EG extraction grid
PG plasma grid
V_e voltage between them
V_s total acceleration voltage
p_s source pressure
p_2 vessel pressure
rf radiofrequency
P_k forward rf power
b. group = beamlet group

Figure 2. 3D geometry of camera setup: (a) section, with z the beam axis; note CAM1 larger tilting (b) overall view, note CAM2 looks to the pump

I. INTRODUCTION and SETUP

An ideal tool to optimize the extraction for a H- ion source would allow to map the beam current density. An approximation to these tool does exist, consisting in vibible light camera [7] observing the Balmer line emission following collision of ions and residual gas. Relevant processes [1, 2] are

$$H^-(\text{fast}) + H_2 \longrightarrow H^-(\text{fast}) + H^* + H^*$$
$$H^-(\text{fast}) + H_2 \longrightarrow H^*(\text{fast}) + H_2 + e$$
$$H^*(n=3) \longrightarrow H^*(n=2) + \gamma(656.28nm)$$

Assuming rapid decay, light emission density is

$L(x, y, z)$ about proportional to $|\mathbf{j}^-_H(\mathbf{x})|$

Since z is the beam axis, method is sensitive to j_z

II.a SETUP

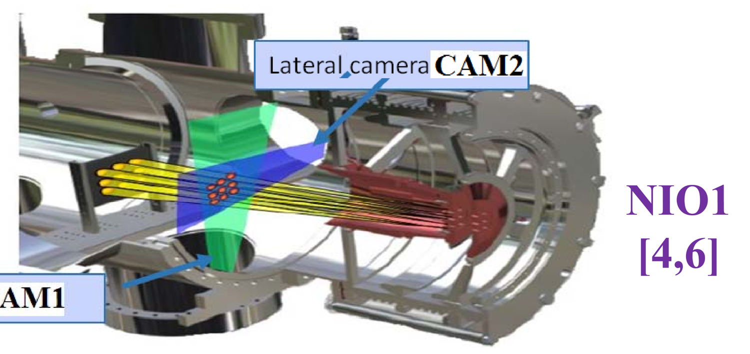

NIO1 (Negative Ion Optimization phase 1) is a H- ion source, producing 9 beamlets. The camera CAM1 and CAM2 must be placed so to avoid: direct view of the plasma; view of brighter reflections. Data can improved by: selecting adequate camera gains; considering as 'data region' only the image portions free from reflections; covering some walls by a black foil.

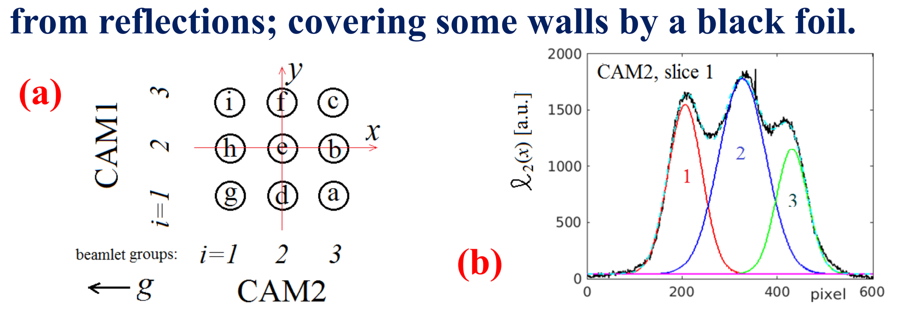

(a) Scheme of beamlet matrix, CAM1 and CAM2 , and their projections, which superpose the 9 beamlets in groups, 1, 2,3 (of course beamlet groups of CAM1 differs from CAM2 ones); (b) fitting peak of CAM1 profiles; with the ambitious purpose of inferring the current contents of beamlet groups.

II.b Typical total currents

In 2019 (Cs-free regime), where most of this poster analysis originates, current was estimated to reach 8-11 mA; with Cs results more than doubled at similar conditions. Here we limited to cases with lower current and better optics, for example the 2019 results have 4 mA current; for some 2022 results see below

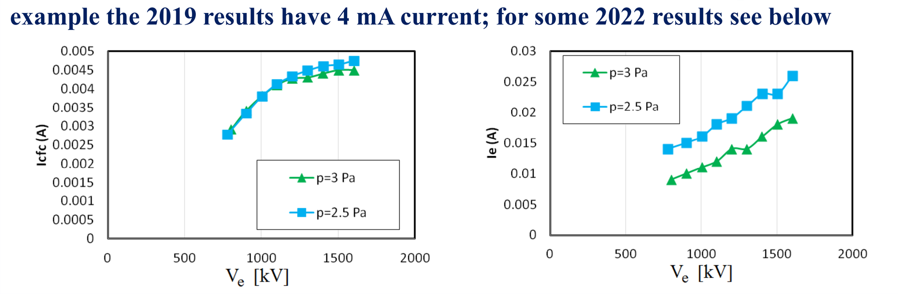

III MODEL FOR FITS

Since x,y ion positions are near z-axis, in 1st approximation we can use a simple light collection model for CAM1 and CAM2

$$\ell_1(z,y) = g_1 \int \mathrm{d}x\ L(x,y,z) \ \propto \int \mathrm{d}x\, j_z(x,y,z) \equiv I_1(z,y)$$
$$\ell_2(z,x) = g_2 \int \mathrm{d}y\ L(x,y,z) \ \propto \int \mathrm{d}y\, j_z(x,y,z) \equiv I_2(z,x) \qquad (3.1)$$

which relates the gains as $g_2 \int \mathrm{d}y \ell_1 = g_1 \int \mathrm{d}x\, \ell_2$

$\bar{\ell}_1(z_k, y)$ indicates average on ±5 pixels, excluding broken pixels.

III.b Primary fits

Since H^- scattering is possible and extraction is complicate, a 3 peak gaussian model was initially tried (+a 4th peak for background)

$$\bar{\ell}_1(z_k, y) \cong \sum_{i=1}^{N} a_i \exp\left(-\frac{(y-b_i)^2}{2\sigma_i^2}\right) \qquad (3.2)$$

$N = 3$ (with label 'fit 3g'

$N = 4$ (with label 'fit 4g' in following pictures)

Background light may include non-gaussian terms, so a polynomial background is often added

$$\bar{\ell}_1(z_k, y) \cong A + By + Cy^2 + \sum_{i=1}^{N} a_i \exp\left(-\frac{(y-b_i)^2}{2\sigma_i^2}\right) \qquad (3.3)$$

For $N = 4$, we must set $C = 0$ (with the label 'fit 4g + 1p')

$N = 3$ we consider (label 'fit 3g + 2p') the Cy^2 term or exclude it ('fit 3g + 1p')

III.c Secondary fits

We expect that b_i (the fitted barycenter of the i-th beamlet group) depends linearly on z_k

So we can consider a linear fit of the z-dependence of the results of the eq. (3.3) fit

$$b_i(z_k) = \alpha_i + \beta_i z_k \quad , \quad \sigma_i(z_k) = \gamma_i + d_i z_k \qquad (3.4)$$

the fit parameters are α_i, β_i, γ_i and the rms divergence d_i

For any b.group we can define the lower and upper border $Y^{\pm}(z)$

$$Y_i^{\pm}(z) = \alpha_i + \beta_i z \pm (\gamma_i + d_i z) \qquad (3.5)$$

III.d Fit implementation notes

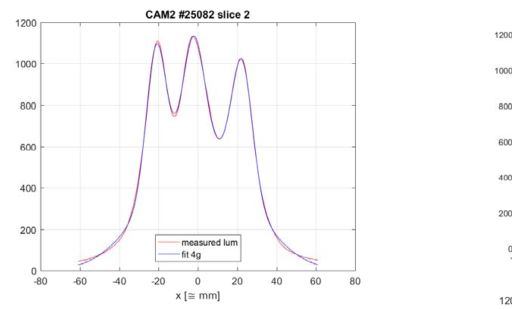

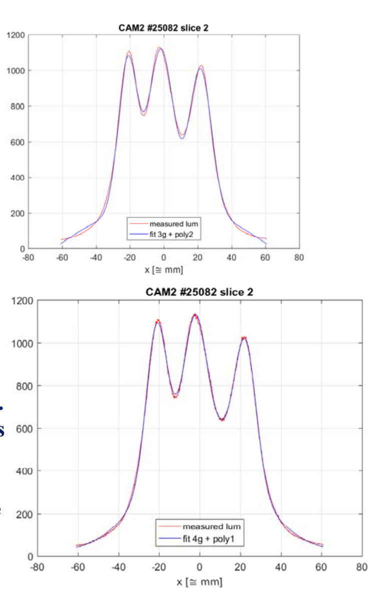

Fitting can be fully automated when the slice profile satisfies a quality check, passed when a search routines find 3 peaks (CAM2 profiles may often give bad cases, CAM1 peaks are typically more separated). This search also give minimal and unbiased constrains for following fits (of course more constrains can be manually imposed). One fit algorithm iteratively relaxes nonlinear parameters in eq 3.3 or eq 3.2, while solving for linear one; this easily converges. More complex algorithm also works.

The 'fit 4g' tends to underestimate tails; the fit 3g+2p tends to overestimate them (see figure above); fit 4g+1p gives typically small errors (compliant with naive error estimate of 10 counts), as in the case shown here above. Anyway, a final choice among these fits is pending and it depends also physical adequacy of results, shown later. In general these fits well perform in typical cases

IV. RESULTS

To perform secondary fit eq. (3.4) we of course need that all slice profiles can be fitted: here an example:

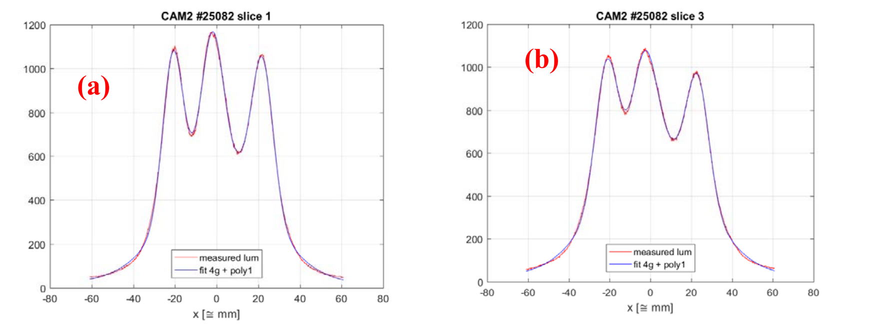

Fitting CAM2 data slices with fit '4g + 1p':(a) slice 1; (b) slice 3.

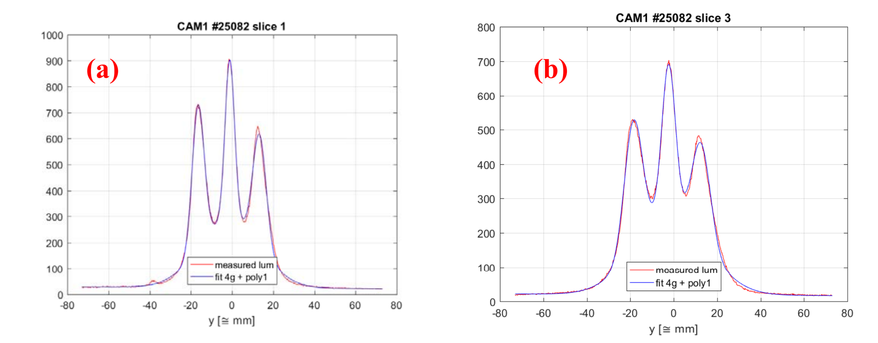

Fitting CAM1 data slices with fit '4g + 1p':(a) slice 1; (b) slice 3

IV.b Result the secondary fits

From secondary fits the rms beam divergence d_i can be calculated for each beamlet group; as well as the beam deflection β_i. A nice graphics of them is the border reconstruction

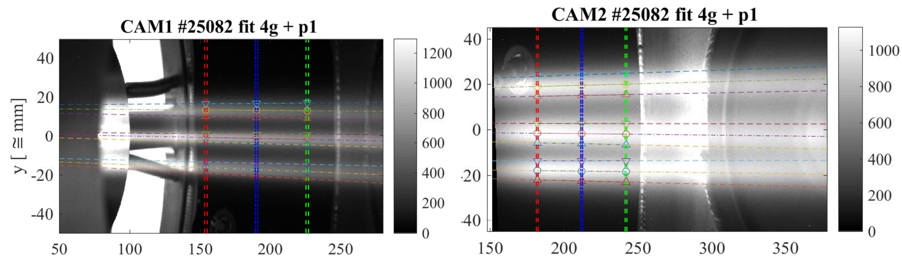

Reconstruction of beamlet borders dataset number 25082 case: CAM1 view and CAM2 view

For same dataset the fit kind '3g+1p' the reconstructed border of the b. group 1 appears to miss the visible image of the 1st b. group (see below); on the contrary the fit '4g+1p' follows image more closely (tentative explanation: fit 4g+1p is more flexible in following profiles. A complete study is under progress)

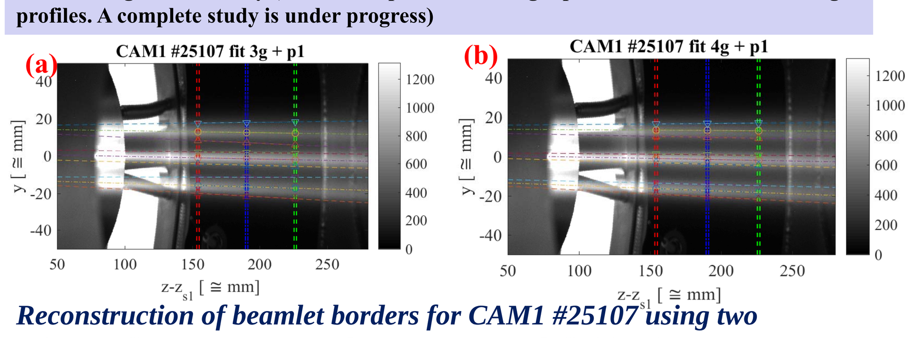

Reconstruction of beamlet borders for CAM1 #25107 using two primary fits: (a) '3g +1p'; (b) '4g+1p' (see definition in eq. 3.3)

IV.c Alternative fits

2D fitting models (where the z surface is used instead of y profile) may offer a valuable and elegant solution to border fits, but with a much greater computational cost; their study is in progress.

IV.d 2022 RESULTS

After the Cs-free result, commission of Cs-oven operation of NIO1 proved very difficult and long (due to pandemic), with some over-cesiation problems. A new pump system allows to operate with larger source pressure p_s and much smaller vessel pressure p_2. CAM1 and CAM2 diagnostics worked smoothly as before, allowing significant comparison and experience. Further calibration are well in progress

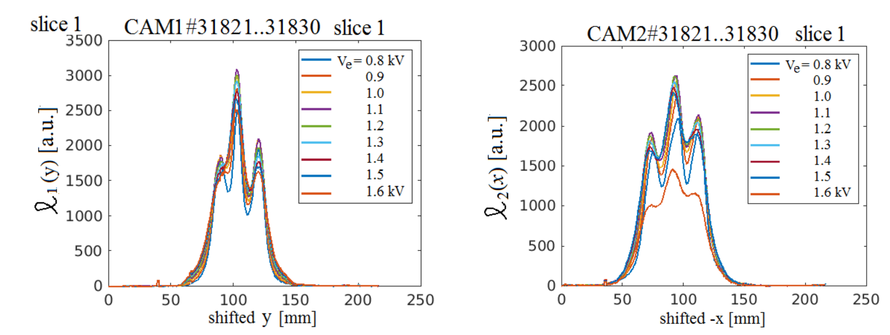

A sample of raw data, with $R_V=V_s/V_e=10$ and V_e as labeled, p_s=1.5 Pa, p_2=12 mPa, rf power P_k=1.6 kW, I_{pg}=400 A, with Cs evaporation.

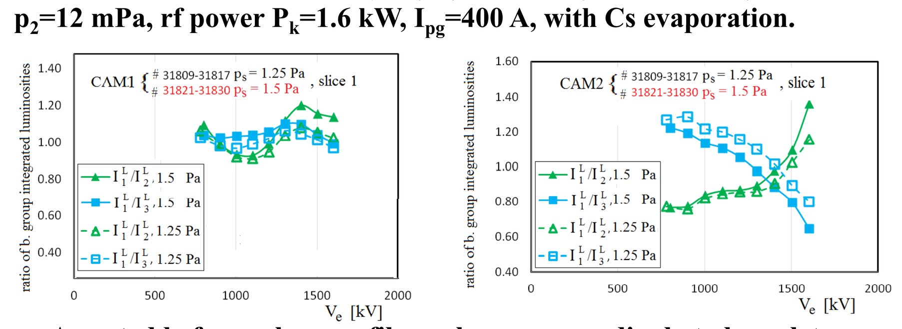

As noted before, when profile peaks correspondingly to beamlet groups are neatly separated (at least in the fit), we approximately consider the peak integrated luminosity I^L_i as proportional to the i-th beamlet group (b. group in brief) current. Figure above show ratios of I^L_i vs voltage V_e, in condition as before; note large variations in CAM2.

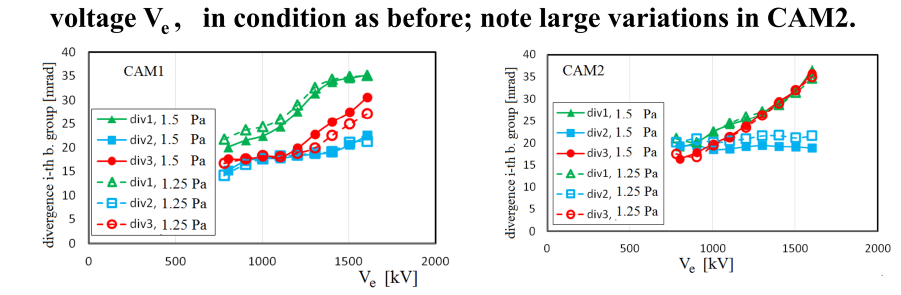

The b. group divergences div_1=1.4 d_1 for the same case as before

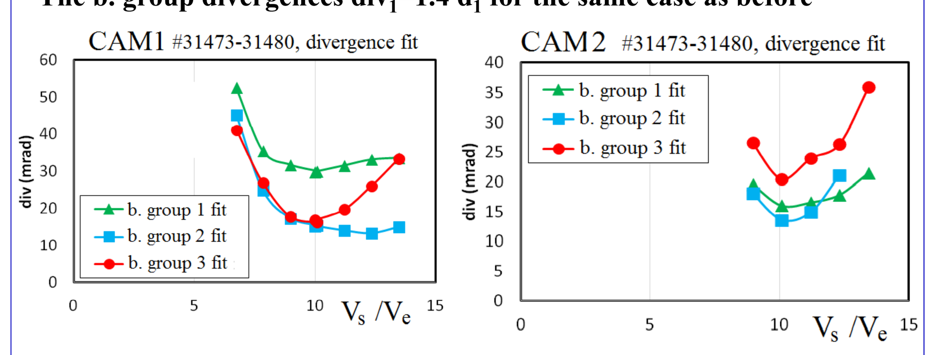

The b. group divergences, now as a function of $R_v=V_s/V_e$. This is most important, for beam optics. Note the typical smile shape, near the minimum at R_v ≈10

V. CONCLUSION

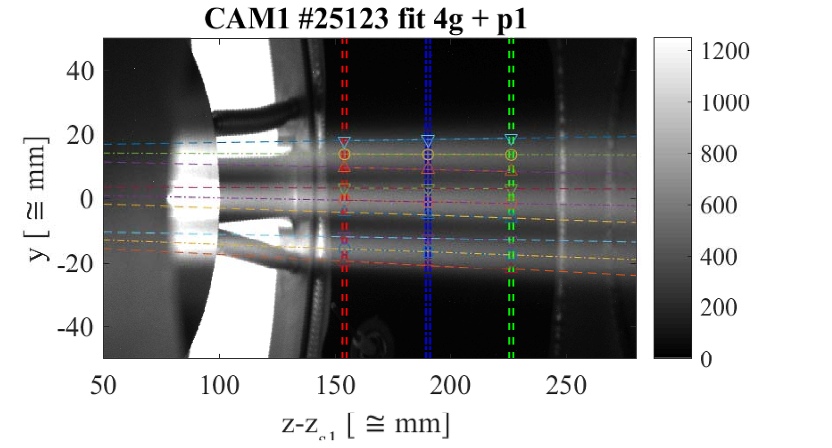

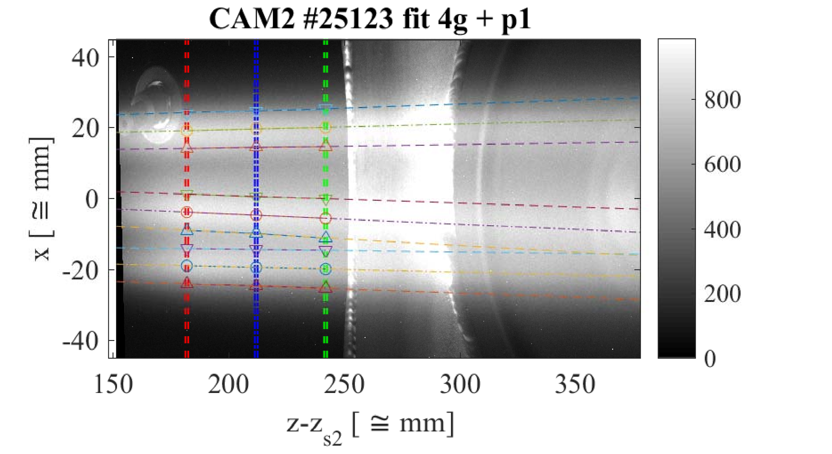

Figure 8. Reconstruction of beamlet borders: (a) CAM1 view (b) CAM2 view; note that extrapolations of beamlet borders 1 and 2 do intersect in front of the pump, as also directly evident from image

The data of NIO1 CAM1 and CAM2 allows to test several fit formula, that were implemented with some attention to practically avoid both over-constrained fit and ill-conditioned fits. While the measurement of current may have perspective of advantages with '3g' fit or 'refit', the border reconstruction clearly show the usefulness of the '4g+1p' fit, perhaps as an additional tools. Beamlet displacement and deviation can be better observed from the border reconstruction, typically based on '4g+1p' fit. In some case, exploration of border reconstruction 'predicts' beamlet groups crossing, directly observed on some CAM2 images. This is consistent with some theoretical approach[5], even if more analysis is surely worthwhile. The crossing of beamlet groups is yet not observed on CAM1, while the data from the new CAM3 being commissioned may allow much more precise observation, at least of deflection in zy plane.

References

[1] M. A. Lieberman and A. J. Lichtenberg, *Principles of Plasma Discharges and Material Processing*, John Wiley, New York, 1994
[2] Taccogna F, Minelli P and Longo S, (2013), Plasma Sources Sci. Technol. 22 045019
[3] Veltri P, Cavenago M and Serianni G, (2014) Rev. Sci. Instrum. 85, 02A711; http://dx.doi.org/10.1063/1.4826075
[4] M. Cavenago, M. Barbisan, R. Delogu, et al., Beam and installation improvements of the NIO1 ion source, Rev. Sci. Instrum. 91, (2020) 013316
[5] M. Cavenago and P. Veltri, Plasma Sources Sci. Technol., 23 (2014) 065024.
[6] M. Cavenago, G. Serianni, C. Baltador, et al., The NIO1 negative ion source: Investigation and operation experience, *AIP Conf. Proc.* 2052, 040013 (2018)
[7] M. Ugoletti, M. Agostini, M. Barbisan et al., Visible cameras as a non-invasive diagnostic to study negative ion beam properties, Rev. Sci. Instrum. 92, 043302 (2021).